JPEDAV (2009) 30:2–11
DOI: 10.1007/s11669-008-9423-8
1547-7037 ©ASM International

Phase Equilibria in the System Al_2O_3-CaO-CoO and Gibbs Energy of Formation of $Ca_3CoAl_4O_{10}$

K.T. Jacob, Chander Shekhar, and G.M. Kale

(Submitted March 10, 2008; in revised form July 30, 2008)

An isothermal section of the system Al_2O_3-CaO-CoO at 1500 K has been established by equilibrating 22 samples of different compositions at high temperature and phase identification by optical and scanning electron microscopy, X-ray diffraction, and energy dispersive spectroscopy after quenching to room temperature. Only one quaternary oxide, $Ca_3CoAl_4O_{10}$, was identified inside the ternary triangle. Based on the phase relations, a solid-state electrochemical cell was designed to measure the Gibbs energy of formation of $Ca_3CoAl_4O_{10}$ in the temperature range from 1150 to 1500 K. Calcia-stabilized zirconia was used as the solid electrolyte and a mixture of Co + CoO as the reference electrode. The cell can be represented as: $(-)Pt, CaAl_2O_4 + Ca_{12}Al_{14}O_{33} + Ca_3CoAl_4O_{10} + Co//(CaO)ZrO_2//CoO + Co, Pt\ (+)$. From the emf of the cell, the standard Gibbs energy change for the $Ca_3CoAl_4O_{10}$ formation reaction, $CoO + 3/5CaAl_2O_4 + 1/5Ca_{12}Al_{14}O_{33} \rightarrow Ca_3CoAl_4O_{10}$, is obtained as a function of temperature: ΔG_r^o/J mol^{-1} (± 50) = $-2673 + 0.289\ (T/K)$. The standard Gibbs energy of formation of $Ca_3CoAl_4O_{10}$ from its component binary oxides, Al_2O_3, CaO, and CoO is derived as a function of temperature. The standard entropy and enthalpy of formation of $Ca_3CoAl_4O_{10}$ at 298.15 K are evaluated. Chemical potential diagrams for the system Al_2O_3-CaO-CoO at 1500 K are presented based on the results of this study and auxiliary information from the literature.

Keywords chemical potential, electromotive force (emf), enthalpy of formation, entropy, experimental thermodynamics, Gibbs energy, ternary phase diagram

1. Introduction

Aluminum is used as a powerful deoxidizer for superalloys based on cobalt. To easily remove solid alumina that forms in the liquid alloy during deoxidation, lime is used as an additive. Because of the occurrence of low liquidus temperatures on either side of the compound $Ca_{12}Al_{14}O_{33}$, alumina can be readily removed from the alloy as a liquid slag. If the initial oxygen content of the alloy is very high, some cobalt oxide (CoO) may be present in the slag phase. It is therefore useful to study the ternary oxide system Al_2O_3-CaO-CoO and identify other complex oxides that may be stable in the system. Cobalt oxide is also used as a coloring agent in ceramic industry.[1] Phase relations in the ternary oxide system is thus of interest in the design of glazes.

The binary systems Al_2O_3-CaO, Al_2O_3-CoO, and CaO-CoO that border the ternary system are well investigated. In the Al_2O_3-CaO system, five phases have been identified ($Ca_3Al_2O_6$, $Ca_{12}Al_{14}O_{33}$, $CaAl_2O_4$, $CaAl_4O_{7,}$, and $CaAl_6O_{10}$) and their thermodynamic property measurements assessed.[2] There is controversy regarding stability of the compound $Ca_{12}Al_{14}O_{33}$. One school of thought considers the phase to be stabilized by moisture or halogens; it is not strictly a stable phase in the binary Al_2O_3-CaO system.[3] The other school considers it as a stable phase in the binary based on thermodynamic and phase equilibrium data.[2,4,5] Cockayne and Lent[6] have grown single crystals of $Ca_{12}Al_{14}O_{33}$ several centimeters long from melt. Although a small infrared absorption band at 2.8 μm corresponding to hydroxyl ions was observed, the intensity was unaffected by prolonged vacuum treatment, suggesting that the hydroxyl ion was present as a minor impurity rather than as a constituent. In the system Ca-Al-O, liquid Al-Ca alloys were found to be in equilibrium with $Ca_{12}Al_{14}O_{33}$ at 1373 K.[7] The experimental data for alloy-oxide equilibrium was in reasonable agreement with thermodynamic calculations. The interoxide phase was also identified as a product during the reduction of CaO by Al under vacuum.[8,9] Since hydroxyl ions would not be stable in the presence of Ca vapor, these results suggest that $Ca_{12}Al_{14}O_{33}$ is stable even in the absence of moisture. The structure of $Ca_{12}Al_{14}O_{33}$ is composed of a positively charged lattice framework, $[Ca_{24}Al_{48}O_{64}]^{4+}$, with 12 subnanometer-sized cages in a cubic unit cell. To maintain charge neutrality, additional O^{2-} ions randomly occupy two of these 12 cages.[10] Various anions (F^-, Cl^-, OH^-, O^-, and O_2^-) can replace O^{2-} ions in the cage.[11-14] Recent results indicate that a part of the O^{2-} ions in the cage can be removed under reducing conditions (carbon container) at high temperatures producing a nonstoichiometric oxide with high electronic conductivity.[15] The X-ray diffraction pattern of

K.T. Jacob, and **Chander Shekhar,** Department of Materials Engineering, Indian Institute of Science, Bangalore 560012, India; **G.M. Kale,** Institute for Materials Research, University of Leeds, Leeds LS2 9JT, UK. Contact e-mail: katob@materials.iisc.ernet.in.

$Ca_{12}Al_{14}O_{33}$ exposed to reducing conditions was almost identical to that of the sample heated in dry oxygen.

The only compound in the system CoO-Al_2O_3 is $CoAl_2O_4$ with spinel structure. The compound can become nonstoichiometric ($CoAl_{2+2x}O_{4+3x}$) by dissolving excess Al_2O_3. The solubility of Al_2O_3 in $CoAl_2O_4$ increases significantly with temperature above 1400 K. There is negligible terminal solid solubility in the pure components below 1573 K. According to Greskovich and Schmalzried,[16] the value of the nonstochiometric parameter x is $\sim 10^{-3}$ at 1423 K and atmospheric pressure of oxygen. A phase diagram for the system CaO-CoO in air was reported by Woermann and Muan.[17] At lower temperatures, compounds with cobalt in the trivalent state are formed ($Ca_3Co_2O_6$, $Ca_3Co_4O_9$, and Co_3O_4). At temperatures above 1300 K, the system exhibits terminal solid solubility at both ends and a two-phase region between CaO-rich solid solution and CoO-rich solid solution.

Vazquez et al.[18] have studied phase relations in the system Al_2O_3-CaO-CoO and determined the crystal structure of the quaternary oxide $Ca_3CoAl_4O_{10}$. A subsolidus phase diagram in air up to a maximum temperature of 1573 K was presented. However, phase-relations in the triangular region bounded by CaO, CoO, and $Ca_3Al_2O_6$ appears to be incorrectly depicted; there are no boundary lines between two-phase and three-phase regions. Their diagrammatic representation violates topological rules of construction of phase diagrams. Further $Ca_3CoAl_4O_{10}$ melts at ~1530 K; liquid phase is not shown on the diagram of Vazquez et al.[18]

The crystal structure of $Ca_3CoAl_4O_{10}$ is orthorhombic with lattice parameters $a = 0.514$ nm, $b = 1.677$ nm, $c = 1.071$ nm, and space group $Pbc2_1$.[18] The compound has an open framework with three crystallographically different channels, each with a diameter of ~0.35 nm.

In the present study, the phase relations in the system Al_2O_3-CaO-CoO were redetermined at 1500 K by isothermal equilibration and phase analysis of 22 compositions. Based on the phase diagram, a solid-state electrochemical cell was designed to measure the standard Gibbs energy of formation of $Ca_3CoAl_4O_{10}$ as a function of temperature. The thermodynamic data can be used for phase diagram computation over a larger range of temperatures and in higher-order systems.

2. Experimental Procedure

2.1 Materials

Fine powders of $CaCO_3$, Al_2O_3, CoO, and Co used in this study were of 99.99% purity. The carbonate and oxides were dried at 673 K before use. Pure compounds $Ca_3Co Al_4O_{10}$, $CaAl_2O_4$,, and $Ca_{12}Al_{14}O_{33}$ required for electrochemical measurements were synthesized by solid-state reaction at 1500 K in flowing dry argon gas. Powders of $CaCO_3$, Al_2O_3, and CoO were intimately mixed in the appropriate stoichiometric proportions by grinding in an agate mortar under acetone. Formation of the quaternary oxide $Ca_3CoAl_4O_{10}$ was sluggish. Attempts to use higher temperatures for synthesis resulted in liquid phase formation at temperatures in excess of 1530 K. The formation of all the interoxide compounds was confirmed by XRD. The XRD pattern of the compound was identical to that reported by Vazquez et al.[18]

High-density impervious calcia-stabilized zirconia solid electrolyte tubes with one end closed were obtained from a commercial source. The tubes were leak tested under vacuum before use. High purity (99.999%) argon gas used in this study was dried by passing over anhydrous silica gel and phosphorus pentoxide, and deoxidized by passing through copper wool at 723 K and titanium sponge at 1123 K prior to use in the experiments.

2.2 Phase Equilibrium Studies

To determine the Al_2O_3-CaO-CoO phase diagram, 22 samples of predetermined compositions were chosen, 6 along the binaries and 16 inside the ternary triangle. To prepare samples for phase equilibrium studies, dried powders of $CaCO_3$, Al_2O_3, and CoO were intimately mixed in predetermined proportions by grinding in acetone. The mixtures contained in Pt crucibles were gradually heated under vacuum up to 900 K to decompose the carbonate. Subsequently, the mixtures were reground, pelletized under dry conditions in a glove box and heated at 1500 K for up to a total of 2 weeks under flowing Ar gas, with intermittent grinding at intervals of 2 days. After each step of heat treatment, the samples were quenched to room temperature. The pellets were then examined by optical and scanning electron microscopy, the phases present were identified by XRD and their compositions determined by energy dispersive spectroscopy (EDS). The heat treatment was stopped when XRD and EDS indicated absence of change in phase composition of the samples after successive heat treatments. The compound $Ca_3CoAl_4O_{10}$ was identified inside the ternary triangle.

2.3 Apparatus for Electrochemical Measurements

Based on the phase relations developed in this study, a solid-state electrochemical cell was designed to measure the standard Gibbs energy of formation of $Ca_3CoAl_4O_{10}$. Advantage was taken of the existence of a three-phase field consisting of $CaAl_2O_4 + Ca_{12}Al_{14}O_{33} + Ca_3CoAl_4O_{10}$. The activity of CoO inside the three-phase field can be determined by equilibrating the three phases with Co metal and then measuring the equilibrium oxygen partial pressure over the four-phase mixture. The reversible emf of the solid-state cell:

$$(-)\ \mathrm{Pt},\ CaAl_2O_4 + Ca_{12}Al_{14}O_{33} + Ca_3CoAl_4O_{10} + \mathrm{Co}//(\mathrm{CaO})ZrO_2//\mathrm{CoO} + \mathrm{Co}, \mathrm{Pt}(+)$$

was measured as a function of temperature. Calcia-stabilized zirconia tube was used as the solid electrolyte and a mixture of $CaAl_2O_4 + Ca_{12}Al_{14}O_{33} + Ca_3CoAl_4O_{10} + Co$ in the molar ratio 1:1:1:1.5 as the working electrode. Each complex oxide in the working electrode was synthesized separately and then mixed with cobalt metal. A schematic diagram of the apparatus is shown in Fig. 1. The four-phase

working electrode was taken inside the solid electrolyte tube. The electrode was formed by ramming an intimate mixture of component powders inside the tube with a Pt lead embedded in the mixture and sintering in situ under flowing Ar gas during the experiments. The reference electrode was prepared by compacting an equimolar mixture of CoO + Co at 100 MPa using a steel die and sintering under prepurified Ar gas at 1473 K. The particle size of the powders used for making the electrodes was in the range from 2 to 6 μm. The two-phase reference electrode pellet was spring loaded against the outside of the flat-bottom solid electrolyte tube by a supporting system of alumina slabs and rods. A thin platinum gauze was placed over the two-phase reference electrode to provide good electrical contact. A platinum lead was spot welded to the gauze.

The assembled cell was enclosed inside a vertical alumina tube closed at both ends with brass heads, which had provisions for spring loading, passage of gases, electrode, and thermocouple leads. The alumina tube was suspended in a vertical resistance furnace. Grounded stainless steel sheet was placed around the outer alumina tube enclosing the cell. The stainless steel cage minimized inductive pick-up from the furnace windings on the cell leads. The cell assembly was situated in the constant-temperature zone (±1 K) of the furnace. The temperature was controlled to ±0.7 K.

Both electrodes were flushed separately with streams of high purity argon gas which was dried and deoxidized prior to their use in the cell. The emf of the cell was measured with a high impedance ($>10^{12}$ Ω) digital voltmeter. The steady-state emf was obtained in 2-15 ks depending on the temperature. The slow response at lower temperatures was probably due to the sluggish kinetics of the reaction involving the four condensed phases.

The reversibility of each cell was checked by passing small currents (~30 μA) through the cell in either direction for 120 s using an external potential source. In each case, the emf was found to return to its original value before the titration. The emf was found to be independent of the flow rate of argon over either electrode in the range of 1-4 mL s^{-1}. The emf was reproducible during the heating and cooling cycles. The temperature of the cell was measured by a Pt/Pt-13% Rh thermocouple placed adjacent to the two-phase reference electrode. The thermocouple was checked against the melting point of Au. The absence of a thermal gradient across the cell was checked by constructing a symmetric cell with identical Co + CoO electrodes. The emf of the symmetric cell was found to be ±0.2 mV over the temperature range from 900 to 1500 K. At the end of the experiment, the pellets were subjected to X-ray diffraction analysis. The phase composition of the electrode pellets was found to be unaltered during the experiment.

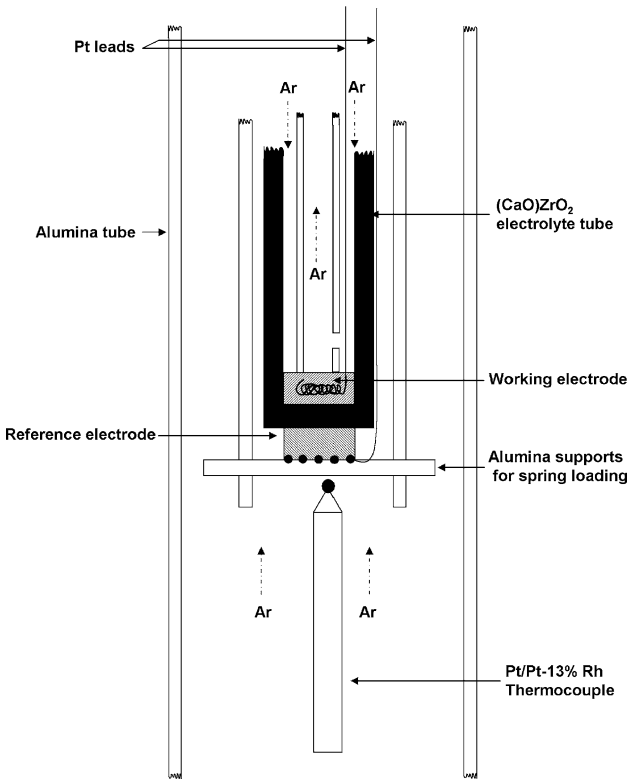

Fig. 1 Schematic diagram of the solid-state galvanic cell

3. Results and Discussion

3.1 Phase Equilibria in the System Al_2O_3-CaO-CoO

The isothermal section of the equilibrium phase diagram for the system Al_2O_3-CaO-CoO at 1500 K, constructed from the results obtained by isothermal equilibration and phase identification of the quenched samples by optical and scanning electron microscopy, XRD and EDS, is shown in the Fig. 2. The summary of experimental information

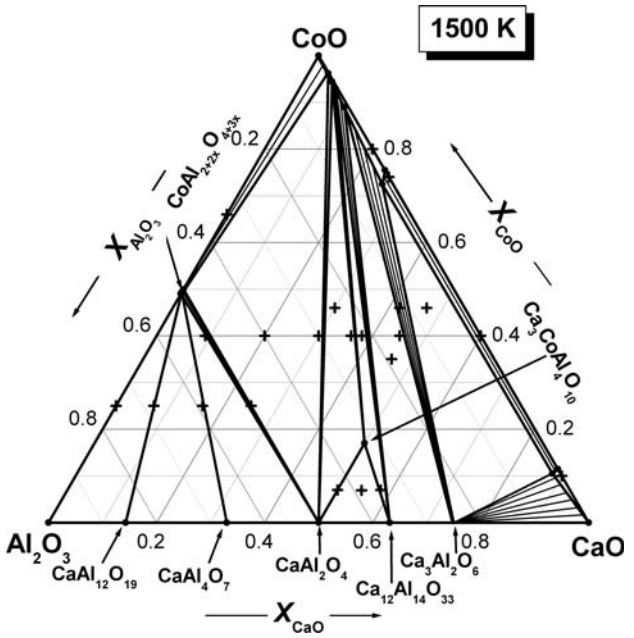

Fig. 2 Isothermal section of equilibrium phase diagram for the system Al_2O_3-CaO-CoO at 1500 K

Table 1 Summary of experimental information regarding phase equilibration studies at 1500 K

Sample number	Average composition			Starting materials	Phases identified	Techniques used
	X_{CaO}	X_{CoO}	$X_{Al_2O_3}$			
1.	0.58	0.07	0.35	Al_2O_3 + CaO + CoO	$Ca_{12}Al_{14}O_{33}$ + $Ca_3CoAl_4O_{10}$	XRD, EDS
2.	0.55	0.07	0.39	Al_2O_3 + CaO + CoO	$Ca_{12}Al_{14}O_{33}$ + $Ca_3CoAl_4O_{10}$ + $CaAl_2O_4$	XRD, EDS
3.	0.50	0.07	0.43	Al_2O_3 + CaO + CoO	$Ca_3CoAl_4O_{10}$ + $CaAl_2O_4$	XRD, EDS
4.	0.90	0.10	0.00	CaO + CoO	CaO_{ss}	XRD, EDS
5.	0.25	0.25	0.50	$CaAl_4O_7$ + CoO	$CaAl_2O_4$ + $CoAl_2O_4$	XRD, EDS
6.	0.25	0.25	0.50	Al_2O_3 + CaO + CoO	$CaAl_2O_4$ + $CoAl_2O_4$	XRD, EDS
7.	0.25	0.25	0.50	$CoAl_2O_4$ + $CaAl_2O_4$	$CaAl_2O_4$ + $CoAl_2O_4$	XRD, EDS
8.	0.16	0.25	0.59	Al_2O_3 + CaO + CoO	$CaAl_4O_7$ + $CoAl_2O_4$	XRD, EDS
9.	0.16	0.25	0.59	$CoAl_2O_4$ + $CaAl_2O_4$	$CaAl_4O_7$ + $CoAl_2O_4$	XRD, EDS
10.	0.07	0.25	0.68	Al_2O_3 + CaO + CoO	$CaAl_{12}O_{19}$ + $CoAl_2O_4$	XRD, EDS
11.	0.07	0.25	0.68	$CoAl_{12}O_{19}$ + $CaAl_2O_4$	$CaAl_{12}O_{19}$ + $CoAl_2O_4$	XRD, EDS
12.	0.00	0.25	0.75	Al_2O_3 + CoO	Al_2O_3 + $CoAl_2O_4$	XRD, EDS
13.	0.46	0.35	0.19	Al_2O_3 + CaO + CoO	$Ca_{12}Al_{14}O_{33}$ + $Ca_3Al_2O_6$ + CoO_{ss}	XRD, EDS
14.	0.60	0.40	0.00	CaO + CoO	CaO_{ss} + CoO_{ss}	XRD, EDS
15.	0.45	0.40	0.15	$Ca_3Al_2O_6$ + CoO	$Ca_3Al_2O_6$ + CoO_{ss}	XRD, EDS (a)
16.	0.45	0.40	0.15	Al_2O_3 + CaO + CoO	$Ca_3Al_2O_6$ + CoO_{ss}	XRD, EDS (a)
17.	0.38	0.40	0.22	$Ca_{12}Al_{14}O_{33}$ + CoO	$Ca_{12}Al_{14}O_{33}$ + $Ca_3CoAl_4O_{10}$ + CoO_{ss}	XRD (b), EDS
18.	0.38	0.40	0.22	Al_2O_3 + CaO + CoO	$Ca_{12}Al_{14}O_{33}$ + $Ca_3CoAl_4O_{10}$ + CoO_{ss}	XRD (b), EDS
19.	0.36	0.40	0.24	Al_2O_3 + CaO + CoO	$Ca_3CoAl_4O_{10}$ + CoO_{ss}	XRD, EDS (c)
20.	0.36	0.40	0.24	$Ca_3CoAl_4O_{10}$ + CoO_{ss}	$Ca_3CoAl_4O_{10}$ + CoO_{ss}	XRD, EDS (c)
21.	0.30	0.40	0.30	$Ca_3Al_2O_6$ + CoO	$CaAl_2O_4$ + CoO_{ss}	XRD, EDS
22.	0.30	0.40	0.30	Al_2O_3 + CaO + CoO	$CaAl_2O_4$ + CoO_{ss}	XRD, EDS
23.	0.20	0.40	0.40	$CaAl_4O_7$ + CoO	$CaAl_2O_4$ + $CoAl_2O_4$ + CoO_{ss}	XRD, EDS
24.	0.20	0.40	0.40	$CoAl_2O_4$ + CaO	$CaAl_2O_4$ + $CoAl_2O_4$ + CoO_{ss}	XRD, EDS
25.	0.20	0.40	0.40	Al_2O_3 + CaO + CoO	$CaAl_2O_4$ + $CoAl_2O_4$ + CoO_{ss}	XRD, EDS
26.	0.09	0.40	0.51	$CaAl_{12}O_{19}$ + CoO	$CaAl_2O_4$ + $CoAl_2O_4$	XRD, EDS
27.	0.09	0.40	0.51	$CoAl_2O_4$ + $CaAl_2O_4$	$CaAl_2O_4$ + $CoAl_2O_4$	XRD, EDS
28.	0.09	0.40	0.51	Al_2O_3 + CaO + CoO	$CaAl_2O_4$ + $CoAl_2O_4$	XRD, EDS
29.	0.47	0.46	0.07	Al_2O_3 + CaO + CoO	CaO_{ss} + CoO_{ss} + $Ca_3Al_2O_6$	XRD, EDS
30.	0.42	0.46	0.12	Al_2O_3 + CaO + CoO	CoO_{ss} + $Ca_3Al_2O_6$	XRD, EDS
31.	0.30	0.46	0.24	Al_2O_3 + CaO + CoO	$Ca_3CoAl_4O_{10}$ + $CaAl_2O_4$ + CoO_{ss}	XRD, EDS
32.	0.00	0.66	0.34	$CaAl_2O_4$ + CoO	$CoAl_2O_4$ + CoO_{ss}	XRD, EDS
33.	0.26	0.74	0.00	CaO + CoO	CoO_{ss} + CaO_{ss}	XRD, EDS
34.	0.20	0.80	0.00	CaO + CoO	CoO_{ss}	XRD, EDS

(a) XRD showed only two phases ($Ca_3Al_2O_6$ + CoO_{ss}). $Ca_{12}Al_{14}O_{33}$ was identified by EDS
(b) XRD signal for $Ca_3CoAl_4O_{10}$ was weak
(c) XRD showed only two phases ($Ca_3CoAl_4O_{10}$ + CoO_{ss}). $CaAl_2O_4$ was identified by EDS

regarding phase equilibration studies is presented in Table 1. Details of 34 samples representing 22 compositions are presented. The equilibrium was assumed when the XRD pattern and EDS showed no change after successive heat treatments. The cross marks indicate the average composition of the samples examined in this study. In several phase fields, equilibrium was confirmed by using different starting materials to produce samples of the same average chemical composition and verifying that the samples had identical phase composition after equilibration. Phase reversal rather than absence of change during equilibration was considered to be decisive to determining phase relationships.

Along the Al_2O_3-CaO binary system, five phases $Ca_3Al_2O_6$, $Ca_{12}Al_{14}O_{33}$, $CaAl_2O_4$, $CaAl_4O_7$, and $CaAl_6O_{10}$ were found to be stable at 1500 K. Since the samples were equilibrated under dry Ar gas, chance of stabilization of oxide phases by hydroxyl ions picked up from atmospheric moisture was minimized. There is extensive terminal solid solubility at both ends in the CaO-CoO binary system. The maximum solubility of CoO in CaO was 11.5 mol% and the solubility limit of CaO in CoO was 24.5 mol%, in reasonable agreement with the data of Woermann and Muan[17] for the binary system. Although there is no detectable solubility of Al_2O_3 in pure CoO and CaO, it increases with concentration in the terminal solid solutions approaching a value of ~1.5 mol% for CaO-rich solid solution at saturation, and ~2.0 mol% for CoO-rich solid solution. Along the Al_2O_3-CoO binary, the only one

interoxide compound $CoAl_2O_4$ with small nonstoichiometry on the Al_2O_3-rich side was detected. The cobalt aluminate has the spinel structure with homogeneity range from 50 to 51 mol% Al_2O_3. Thus the maximum value of the nonstoichiometric parameter x in the spinel $CoAl_{2+2x}O_{4+3x}$ is 0.04 at 1500 K.

The isothermal section in Fig. 2 contains nine three-phase regions and eight extended two-phase regions. Seven of the extended two-phase regions involve the solid solutions based on CaO or CoO and the eighth involves the nonstoichiometric spinel phase. Other two-phase equilibria, in which both phases have essentially fixed composition, are shown on the diagram by straight lines connecting the two phases. Cobalt aluminate ($CoAl_{2+2x}O_{4+3x}$) is stable in contact with three calcium aluminates on the Al_2O_3-rich side, $CaAl_2O_4$, $CaAl_4O_7$, and $CaAl_6O_{10}$, and with CoO-rich solid solution. Three calcium aluminates on the CaO-rich side, $Ca_3Al_2O_6$, $Ca_{12}Al_{14}O_{33}$, and $CaAl_2O_4$ are in equilibrium with CoO solid solutions of different compositions. The quaternary oxide $Ca_3CoAl_4O_{10}$ is in stable contact with only a small range of CoO solid solution, $Ca_{12}Al_{14}O_{33}$, and $CaAl_2O_4$. The compositions across the miscibility gap near the binary CaO-CoO form a three-phase region with CaO-rich aluminate, $Ca_3Al_2O_6$. The three-phase region containing $Ca_{12}Al_{14}O_{33}$ + $CaAl_2O_4$ + $Ca_3CoAl_4O_{10}$ offers a convenient method for the measurement of Gibbs energy of formation of $Ca_3CoAl_4O_{10}$. In this phase field CoO exists at reduced activity. The activity of CoO can be determined by equilibrating the mixture of three oxides with metallic Co and then measuring the equilibrium oxygen partial pressure. Oxygen-ion conducting solid electrolytes provides a means for accurate measurement of oxygen partial pressure.

The isothermal section of the ternary oxide system Al_2O_3-CaO-CoO at 1500 K established in this study is qualitatively similar to the nonisothermal subsolidus phase relations below 1573 K reported by Vazquez et al.,[18] but the two diagrams differ in significant details. According to the phase diagram proposed by Vazquez et al.,[18] the three calcium aluminates, $Ca_3Al_2O_6$, $Ca_{12}Al_{14}O_{33}$, and $CaAl_2O_4$, coexist with essentially pure CoO (although the compositions were not determined), whereas in this study they were found to be in equilibrium with CoO solid solutions. Further results of this study indicate that $CoAl_2O_4$ is in equilibrium with a small range of CoO-rich solid solutions, whereas Vazquez et al.[18] display equilibrium with essentially pure CoO. Thus the diagram shown in Fig. 2 can be considered as a refinement of the diagram available in the literature.[18] Figure 2 is valid from one atmosphere pressure of diatomic oxygen gas down to the partial pressure of oxygen corresponding to the dissociation of CoO; $1.2 \times 10^{-9} \leq P_{O_2}/P^o \leq 1$ at 1500 K, where P^o is the standard atmospheric pressure (1.013×10^5 Pa).

3.2 Gibbs Energy of Formation of $Ca_3CoAl_4O_{10}$

The reversible emf of the solid-state electrochemical cell, $(-)$ Pt, $CaAl_2O_4 + Ca_{12}Al_{14}O_{33} + Ca_3CoAl_4O_{10} + Co$// $(CaO)ZrO_2$//$CoO + Co$, Pt$(+)$ is shown in Fig. 3 as a function of temperature from 1150 to 1500 K. The linear least square regression analysis gives:

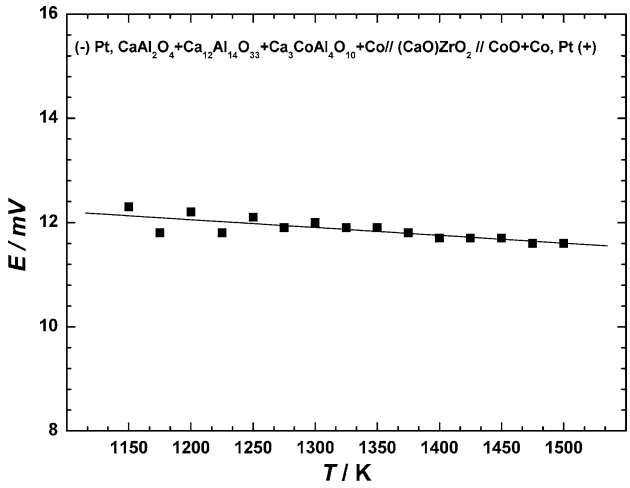

Fig. 3 Variation of the reversible emf of the solid-state electrochemical cell as a function of temperature

$$E/\text{mV}\ (\pm 0.26) = 13.85 - 0.0015\ (T/\text{K}) \qquad \text{(Eq 1)}$$

where the uncertainty limit corresponds to twice the standard error estimate (2σ). The emf of the cell is related to the standard Gibbs energy change for the cell reaction:

$$CoO + 3/5CaAl_2O_4 + 1/5Ca_{12}Al_{14}O_{33} \rightarrow Ca_3CoAl_4O_{10} \qquad \text{(Eq 2)}$$

$$\Delta G^o_{r(2)}/\text{J mol}^{-1}(\pm 50) = -\eta F E = -2673 + 0.289\ (T/\text{K}) \qquad \text{(Eq 3)}$$

where F is the Faraday constant and $\eta = 2$ is the number of electrons involved in the electrode reactions per mole of $Ca_3CoAl_4O_{10}$. The electrochemical measurements give an accurate value for the Gibbs energy change for reaction 2. The Gibbs energy of formation of $Ca_3CoAl_4O_{10}$ from the two calcium aluminates and CoO is rather small and decreases with increasing temperature. Because of the marginal stability in relation to its neighboring phases on the Gibbs triangle and the relatively low melting point, primary phase field of crystallization of $Ca_3CoAl_4O_{10}$ is likely to be very restricted or nonexistent.

The oxygen chemical potential at the working electrode of the cell defined by the equation,

$$Co + 1/2O_2 + 3/5CaAl_2O_4 + 1/5Ca_{12}Al_{14}O_{33} \rightarrow Ca_3CoAl_4O_{10} \qquad \text{(Eq 4)}$$

can be computed from the emf and the oxygen potential of the reference electrode.[19]

$$\Delta\mu_{O_2}/\text{J mol}^{-1}(\pm 115) = 2\Delta G^o_{r(4)} = -474586 + 142.618\ (T/\text{K}) \qquad \text{(Eq 5)}$$

The standard Gibbs energy of formation of $Ca_3CoAl_4O_{10}$ from the binary oxides can be calculated using (Eq 3) and

the Gibbs energies of formation of the two calcium aluminates $CaAl_2O_4$ and $Ca_{12}Al_{14}O_{33}$ available in the literature.[2] The standard Gibbs energies of formation of $CaAl_2O_4$ and $Ca_{12}Al_{14}O_{33}$ from their component binary oxides can be represented by the following expressions:

$$CaO + Al_2O_3(\alpha) \rightarrow CaAl_2O_4 \quad \text{(Eq 6)}$$

$$\Delta G^{o}_{f,ox}(CaAl_2O_4)/\text{J mol}^{-1}(\pm 1500) = -18120 - 18.62\ (T/\text{K}) \quad \text{(Eq 7)}$$

and

$$12CaO + 7Al_2O_3(\alpha) \rightarrow Ca_{12}Al_{14}O_{33} \quad \text{(Eq 8)}$$

$$\Delta G^{o}_{f,ox}(Ca_{12}Al_{14}O_{33})/\text{J mol}^{-1}(\pm 17500) = -86100 - 205.1\ (T/\text{K}) \quad \text{(Eq 9)}$$

Using the Gibbs energies of formation of $CaAl_2O_4$ and $Ca_{12}Al_{14}O_{33}$, the standard Gibbs energy of formation of $Ca_3CoAl_4O_{10}$ from its constituent binary oxides according to the reaction,

$$3CaO + CoO + 2\ Al_2O_3(\alpha) \rightarrow Ca_3CoAl_4O_{10} \quad \text{(Eq 10)}$$

is obtained as,

$$\Delta G^{o}_{f,ox}(Ca_3CoAl_4O_{10})/\text{J mol}^{-1}(\pm 3700) = -30765 - 51.09\ (T/\text{K}) \quad \text{(Eq 11)}$$

The relatively larger uncertainty associated with (Eq 11), arises mainly from uncertainties associated with data of the two calcium aluminates. When more reliable information becomes available for calcium aluminates, a more accurate expression can be derived for the standard Gibbs energy of formation of $Ca_3CoAl_4O_{10}$ from binary oxides. The temperature-independent term in (Eq 11) represents the value of enthalpy of formation from component binary oxides $\{\Delta H^{o}_{f,ox}\ (Ca_3CoAl_4O_{10})/\text{kJ mol}^{-1}\ (\pm 4.5) = -30.77\}$ at an average temperature of 1325 K. The temperature-dependent term in Eq 11 with sign reversed gives the corresponding entropy change: $\Delta S^{o}_{f,ox}(Ca_3CoAl_4O_{10})/\text{J mol}^{-1}\ \text{K}^{-1}(\pm 3.4) = 51.09$. Applying the Neumann-Kopp rule for estimating the heat capacity of $Ca_3CoAl_4O_{10}$ and combining with the standard enthalpy and entropy of formation of binary oxides given in NIST-JANAF tables,[20] the standard entropy of $Ca_3CoAl_4O_{10}$ at 298.15 K can be estimated as $S^{o}_{298.15}/\text{J mol}^{-1}\ \text{K}^{-1}\ (\pm 3.5) = 321.4$ and standard enthalpy of formation of $Ca_3CoAl_4O_{10}$ from elements in their normal standard states at 298.15 K as $\Delta H^{o}_{f,298.15}/\text{kJ mol}^{-1}\ (\pm 5.8) = -5525.2$.

In principle, the measured thermodynamic data for $Ca_3CoAl_4O_{10}$ can be cross checked by determining the activity of CaO in the three-phase field CoO + $CaAl_2O_4$ + $Ca_3CoAl_4O_{10}$ using a solid-state cell based on single-crystal CaF_2 as the electrolyte. Unfortunately the response of the cell based on CaF_2 was too sluggish for this attempt to be successful. From a philosophical point of view, it is interesting to compare the progression in the scale of energetics in going from binary to ternary and quaternary oxides. The average value of the Gibbs energy of formation of the binary oxides (CaO, CoO, and Al_2O_3) per gram atom of oxygen is -334.3 kJ (g at. O)$^{-1}$. The average value of the Gibbs energy of formation of the ternary oxides ($Ca_3Al_2O_6$, $Ca_{12}Al_{14}O_{33}$, $CaAl_2O_4$, $CaAl_4O_7$, $CaAl_6O_{10}$, and $CoAl_2O_4$) from their component binary oxides is -7.16 kJ (g at. O)$^{-1}$. The Gibbs energy of formation of the quaternary oxide $Ca_3CoAl_4O_{10}$ from its surrounding oxides on the phase diagram ($CaAl_2O_4$, $Ca_{12}Al_{14}O_{33}$, and CoO) is -0.224 kJ (g at. O)$^{-1}$. Thus there is a dramatic decrease in the energies of interaction as one proceeds from the binary to higher order systems. Similar trends were observed in earlier studies on the systems CaO-MO-SiO_2 (M = Co, Ni).[21,22]

3.3 Chemical Potential Diagrams

The stability domain of different phases at constant temperature and total pressure can be depicted in two dimensions by plotting the chemical potential of one of the components of the pseudo-ternary system as a function of the normalized mole fraction of the other two components. The composition of a component is normally designated by its mole fraction, which is obtained by dividing the number of moles of the component with the sum of moles of all components. The normalized mole fraction, used as the composition variable in chemical-potential diagrams, is obtained by removing the component, the chemical potential of which is being plotted, from the summation in the denominator. Thus, the chemical potential becomes an independent variable with respect to the normalized mole fraction.

The variation of the chemical potentials of Al_2O_3, CaO, and CoO with the corresponding normalized mole fractions in the Al_2O_3-CaO-CoO system at 1500 K and standard pressure are shown in the Fig. 4-6. The diagrams are calculated using the Gibbs energy of formation of the quaternary phase ($Ca_3CoAl_4O_{10}$) determined in the present study, data for CaO-CoO solid solution estimated from the miscibility gap boundaries, and Gibbs energies of formation of calcium aluminates ($CaAl_{12}O_{19}$, $CaAl_4O_7$, $CaAl_2O_4$, $Ca_{12}Al_{14}O_{33}$, and $Ca_3Al_2O_6$) and cobalt aluminate spinel ($CoAl_2O_4$) from the literature.[2,24,25] The data are summarized in Table 2. The small nonstoichiometry of the spinel phase is ignored in the calculations. When three condensed phases coexist at constant temperature and pressure, the chemical potential is invariant and can be represented by a horizontal line on the diagrams. The diagrams obey the same topological rules of construction that are applicable to the more familiar temperature-composition (*T-X*) phase diagrams. The chemical potential diagrams provide complimentary information regarding phase equilibria which are conventionally represented on the Gibbs ternary triangle (Fig. 2). The diagrams show the variation of the chemical potential of an apex species as one proceeds from the binary system represented by a side of the ternary triangle toward the opposite apex.

In the pseudo-binary system CaO-CoO, there exist terminal solid solutions depicted as CaO_{ss} and CoO_{ss}, separated by a two-phase region CaO_{ss} + CoO_{ss}. Since the terminal solid solutions have the same crystal structure, the

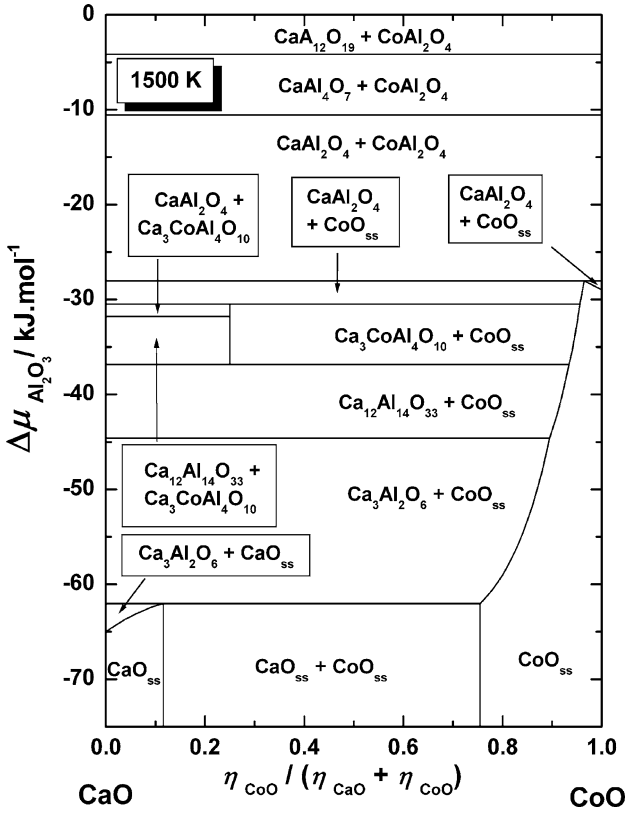

Fig. 4 Chemical potential of Al_2O_3 in the system Al_2O_3-CaO-CoO at 1500 K

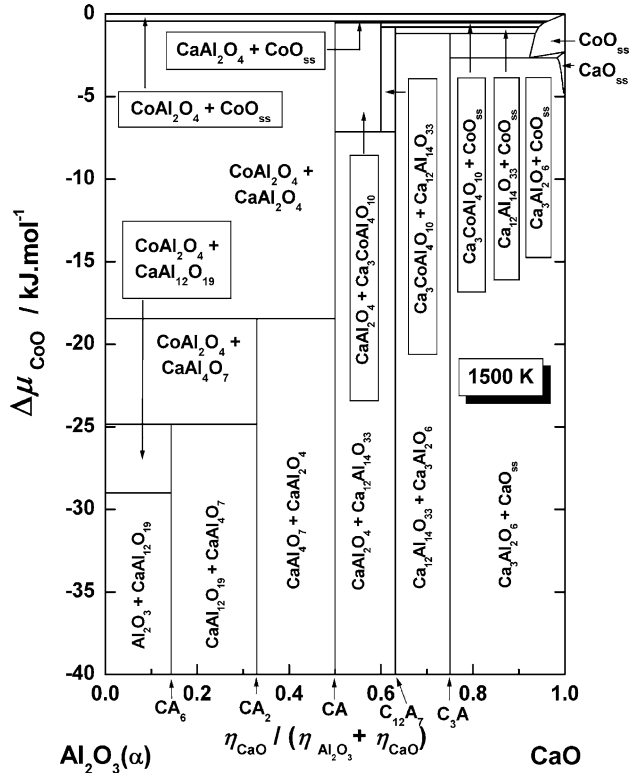

Fig. 5 Chemical potential of CoO in the system Al_2O_3-CaO-CoO at 1500 K

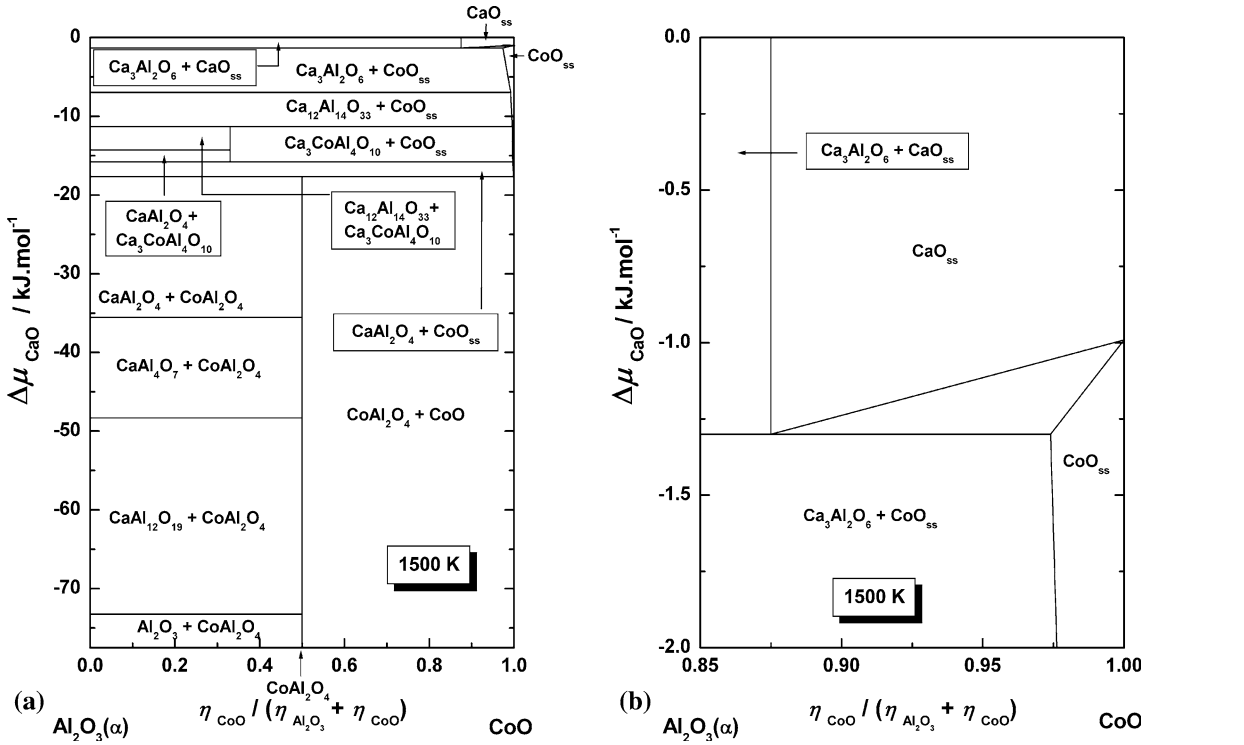

Fig. 6 (a) Chemical potential of CaO in the system Al_2O_3-CaO-CoO at 1500 K. (b) Enlarged view of the chemical potential diagram (Fig. 6a) showing the two-phase region CaO_{ss} + CoO_{ss}

Table 2 Energy of formation of the compounds from component binary oxides

No.	Compound	Free energy (kJ mol^{-1})	Temperature range (K)	Reference
1.	$CaAl_2O_{19}$	$-17{,}430 - 37.2T$ ($\pm$1500)	923-1900	Allibert et al.[2]
2.	$CaAl_4O_7$	$-16{,}400 - 26.8T$ ($\pm$2500)	923-1900	Allibert et al.[2]
3.	$CaAl_2O_4$	$-18{,}120 - 18.62T$ ($\pm$1500)	923-1900	Allibert et al.[2]
4.	$Ca_{12}Al_{14}O_{33}$	$-86{,}100 - 205.1T$ ($\pm$17,500)	923-1600	Allibert et al.[2]
5.	$Ca_3Al_2O_6$	$-17{,}000 - 32.0T$ ($\pm$1500)	923-1800	Allibert et al.[2]
6.	$CoAl_2O_4$	$-30{,}430 + 0.96T$ ($\pm$600)	900-1500	Jacob and Hajra[24] and Jacob[25]
7.	$Ca_3CoAl_4O_{10}$	$-30{,}765 - 51.09T$ ($\pm$1700)	1150-1500	This study

Table 3 Reactions and corresponding chemical potentials of Al_2O_3 at 1500 K in the system Al_2O_3-CaO-CoO

No.	Reactions defining $\Delta\mu_{Al_2O_3}$	Composition of (CaO-CoO-Al_2O_3)$_{ss}$ $\eta_{CoO}/(\eta_{CoO}+\eta_{CaO})$	$\Delta\mu_{Al_2O_3}$ (1500 K), kJ/mol
1	$1/4CaAl_4O_7 + Al_2O_3 \rightarrow 1/4CaAl_2O_{19}$	...	−04.16
2	$CaAl_2O_4 + Al_2O_3 \rightarrow CaAl_4O_7$	...	−10.55
3	$CoO_{ss} + Al_2O_3 \rightarrow CoAl_2O_4$	0.964	−28.02
		1	−28.90
4	$Ca_3CoAl_4O_{10} + Al_2O_3 \rightarrow 3CaAl_2O_4 + CoO_{ss}$	0.956	−30.48
5	$1/5Ca_{12}Al_{14}O_{33} + Al_2O_3 \rightarrow 12/5CaAl_2O_4$	...	−31.77
6	$Ca_{12}Al_{14}O_{33} + 4CoO_{ss} + Al_2O_3 \rightarrow 4Ca_3CoAl_4O_{10}$	0.934	−36.84
7	$4/3Ca_3Al_2O_6 + Al_2O_3 \rightarrow 1/3Ca_{12}Al_{14}O_{33}$	0.8947	−44.6
8	$3CaO_{ss} + Al_2O_3 \rightarrow Ca_3Al_2O_6$	0.115/0.754	−62.05
		0.07	−62.89
		0.03	−63.97
		0	−65.00

two-phase region must be the result of large positive enthalpy of mixing. The region of immiscibility is asymmetric and extends from $X_{CoO} = 0.115$ to $X_{CoO} = 0.755$ at 1500 K. The mixing properties of the solid solution, $Ca_xCo_{(1-x)}O$, in the CaO-CoO system can be derived from the miscibility gap data. The activity of each component is the same in the two phases in equilibrium. Since the immiscibility gap is assymmetric, the simplest thermodynamic model that can reproduce the data is the sub-regular solution model of Hardy.[23] The excess Gibbs energy of mixing in this model can be represented as:

$$\Delta G^{E}/\text{J mol}^{-1} = X_{CaO}X_{CoO}(AX_{CaO} + BX_{CoO}) \quad \text{(Eq 12)}$$

The expression is equivalent to the truncated Redlich-Kister empirical equation with two coefficients. The activities of the end members are then given by:

$$a_{CaO} = X_{CaO}\exp((1 - X_{CaO})^2((2A - B) + 2(1 - X_{CaO})(B - A))/RT) \quad \text{(Eq 13)}$$

$$a_{CoO} = (1 - X_{CaO})\exp(X_{CaO}^2((2B - A) + 2X_{CaO}(A - B))/RT) \quad \text{(Eq 14)}$$

The sub-regular solution constants A and B are determined at 1500 K by solving the equations,

$$a_{CoO}|_{X_{CoO}=0.115} = a_{CoO}|_{X_{CoO}=0.755} \quad \text{(Eq 15)}$$

$$a_{CaO}|_{X_{CaO}=0.115} = a_{CaO}|_{X_{CaO}=0.755} \quad \text{(Eq 16)}$$

where the activities are defined by Eqs 13 and 14. The values obtained are A/J mol^{-1} = 33,544 and B/J mol^{-1} = 24,702.

The variation of the chemical potential of Al_2O_3 with the normalized mole fraction, $\eta_{CoO}/(\eta_{CoO} + \eta_{CaO})$, in the ternary system CoO-CaO-Al_2O_3 at 1500 K is shown in the Fig. 4. The standard state for Al_2O_3 is the α form. The chemical potential is constant (horizontal line) when three condensed phases coexist. The reactions defining the chemical potential of Al_2O_3 are summarized in Table 3. The chemical potential of Al_2O_3 is zero in the three-phase field that contains pure Al_2O_3 ($CaAl_{12}O_{19}$ + $CoAl_2O_4$ + Al_2O_3). Only the single (except line compounds) and two-phase fields are labeled on the diagram. For phase fields involving a solid solution [CaO_{ss} + $Ca_3Al_2O_6$, CoO_{ss} + $Ca_3Al_2O_6$, $Ca_{12}Al_{14}O_{33}$ + CoO_{ss}, $Ca_3CoAl_4O_{10}$ + CoO_{ss}, and $CaAl_2O_4$ + CoO_{ss}], their curved boundaries are calculated from the activity of CaO in the solid solution corresponding to specific values of chemical potential of Al_2O_3. It is seen from the diagram that the quaternary oxide $Ca_3CoAl_4O_{10}$ is stable only in a narrow range of chemical potential.

Table 4 Reactions and corresponding chemical potentials of CoO at 1500 K in the system Al_2O_3-CaO-CoO

No.	Reactions defining $\Delta\mu_{CoO}$	Composition of $(CaO\text{-}CoO\text{-}Al_2O_3)_{ss}$ $\eta_{CaO}/(\eta_{Al_2O_3}+\eta_{CaO})$	$\Delta\mu_{CoO}$ (1500 K), kJ/mol
1	$CaAl_2O_4 + CoO \rightarrow CoAl_2O_4 + CaO_{ss}$	0.966	−0.44
2	$2CaAl_2O_4 + CoO + CaO_{ss} \rightarrow Ca_3CoAl_4O_{10}$	0.946	−0.52
3	$2/7Ca_{12}Al_{14}O_{33} + CoO \rightarrow Ca_3CoAl_4O_{10} + 3/7CaO_{ss}$	0.943	−0.78
4	$7/9Ca_3Al_2O_6 \rightarrow 1/9Ca_{12}Al_{14}O_{33} + CaO_{ss}$	0.936	−1.18
5	$CoO \rightarrow CoO_{ss}$ (a)	1	−2.29
		0.923/0.983	−2.65
6	$1/5Ca_{12}Al_{14}O_{33} + 3/5CaAl_2O_4 + CoO \rightarrow Ca_3CoAl_4O_{10}$	···	−7.13
7	$CaAl_4O_7 + CoO \rightarrow CoAl_2O_4 + CaAl_2O_4$	···	−18.44
8	$1/5CaAl_{12}O_{19} + CoO \rightarrow CoAl_2O_4 + 1/5CaAl_2O_4$	···	−24.83
9	$Al_2O_3 + CoO \rightarrow CoAl_2O_4$	···	−28.99

(a) Two-phase region $CoO_{ss} + CaO_{ss}$

Table 5 Reactions and corresponding chemical potentials of CaO at 1500 K in the system Al_2O_3-CaO-CoO

No.	Reactions defining $\Delta\mu_{CaO}$	Composition of $(CaO\text{-}CoO\text{-}Al_2O_3)_{ss}$ $\eta_{CoO}/(\eta_{Al_2O_3}+\eta_{CoO})$	$\Delta\mu_{CaO}$ (1500 K), kJ/mol
1	$CaO \rightarrow CaO_{ss}$ (a)	1	−0.99
		0.974	−1.30
2	$1/9Ca_{12}Al_{14}O_{33} + CaO \rightarrow 7/9Ca_3Al_2O_6$	0.992	−6.94
3	$7/3Ca_3CoAl_4O_{10} + CaO \rightarrow 2/3Ca_{12}Al_{14}O_{33} + 7/3CoO_{ss}$	0.996	−11.29
4	$7/5CaAl_2O_4 + CaO \rightarrow 1/5Ca_{12}Al_{14}O_{33}$	···	−14.29
5	$CoO_{ss} + 2CaAl_2O_4 + CaO \rightarrow Ca_3CoAl_4O_{10}$	0.997	−15.77
6	$CoAl_2O_4 + CaO \rightarrow CaAl_2O_4 + CoO_{ss}$	0.999	−17.68
7	$CaAl_4O_7 + CaO \rightarrow 2CaAl_2O_4$	···	−35.53
8	$1/2CaAl_{12}O_{19} + CaO \rightarrow 3/2CaAl_4O_7$	···	−48.30
9	$6Al_2O_3 + CaO \rightarrow CaAl_{12}O_{19}$	···	−73.23

(a) Two-phase region $CoO_{ss} + CaO_{ss}$

Displayed in Fig. 5 is the variation of the chemical potential for CoO with the normalized mole fraction $\eta_{CaO}/(\eta_{Al_2O_3}+\eta_{CaO})$ at 1500 K. The reactions that define the chemical potential of CoO are listed in Table 4. Except when solid solutions are involved, two-phase fields are bounded by horizontal and vertical lines. Since the solubility of Al_2O_3 in solid solutions based on CoO and CaO is low, the solid solution single phase fields do not appear prominent on the diagram. Presented in Fig. 6a is the variation of the chemical potential of CaO with the normalized mole fraction $\eta_{CoO}/(\eta_{Al_2O_3}+\eta_{CoO})$ at 1500 K. An enlarged view of the two-phase region involving the two monoxide solid solutions is presented in Fig. 6(b). The reactions that define the chemical potential of CaO are listed in Table 5. Similar diagrams at other temperatures can be readily computed from the thermodynamic information now available.

4. Conclusions

The isothermal section of the phase diagram of the system Al_2O_3-CaO-CoO at 1500 K has been established by phase analysis of the samples quenched after equilibration at high temperature. Only one quaternary compound $Ca_3CoAl_4O_{10}$ was detected. The standard Gibbs energy of formation of $Ca_3CoAl_4O_{10}$ was determined using a solid-state electrochemical cell. The measurements give accurate values for the Gibbs energy of formation of $Ca_3CoAl_4O_{10}$ from the two calcium aluminates ($CaAl_2O_4$ and $Ca_3CoAl_4O_{10}$) and CoO; for the reaction, $CoO + 3/5CaAl_2O_4 + 1/5Ca_{12}Al_{14}O_{33} \rightarrow Ca_3CoAl_4O_{10}$, $\Delta G_r^o/J\ mol^{-1}(\pm 50) = -2673 + 0.289\ (T/K)$. For the formation of the quaternary oxide from its component binary oxides according to the reaction, $3CaO + CoO + 2Al_2O_3 \rightarrow Ca_3CoAl_4O_{10}$, $\Delta G_{f,ox}^o$

$(Ca_3CoAl_4O_{10})$/J mol^{-1} ($\pm$3700) = $-30765 - 51.90$ (T/K). The obtained thermodynamic information can be included in the thermodynamic databases and the various kinds of phase diagrams can be calculated in a range of temperature and oxygen partial pressures, which have not been experimentally studied so far. Chemical potential diagrams are computed for the system Al_2O_3-CaO-CoO at 1500 K based on the results obtained in this study and thermodynamic information on ternary oxides available in the literature. The chemical potential diagrams provide information on the stability domain of each phase that is complimentary to Gibbs triangle representation of phase relations.

References

1. J. Alarcon, P. Escribano, and R.M. Martin, Cobalt (II) Based Ceramic Pigments, *Trans. Br. Ceram. Soc.*, 1985, **84**(5), p 170-172
2. M. Allibert, C. Chatillon, K.T. Jacob, and R. Lourtau, Mass-Spectrometric and Electrochemical Studies of Thermodynamic Properties of Liquid and Solid Phases in the System CaO-Al_2O_3, *J. Am. Ceram. Soc.*, 1981, **64**(5), p 307-314
3. R.W. Nurse, J.H. Welch, and A.J. Majumdar, The CaO- Al_2O_3 System in a Moisture-free Atmosphere, *Trans. Br. Ceramic Soc.*, 1965, **64**(9), p 409-418
4. R.G.J. Ball, M.A. Mignanelli, T.I. Barry, and J.A. Gisby, The Calculation of Phase Equilibria of Oxide Core-concrete Systems, *J. Nucl. Mater.*, 1993, **201**, p 238-249
5. A.K. Chatterjee and G.I. Zhmoidin, The Phase Equilibrium Diagram of the System CaO-Al_2O_3-CaF_2, *J. Mater. Sci.*, 1972, **7**(1), p 93-97
6. B. Cockayne and B. Lent, Single Crystal Growth of 12CaO $7Al_2O_3$, *J. Cryst. Growth*, 1979, **46**(4), p 467-473
7. S. Srikanth, V.S. Srinivasan, K.T. Jacob, and M. Allibert, Alloy-Oxide Equilibria in the System Ca-Al-O at 1373 K, *Rev. Int. Htes. Temp. Refract.*, 1991, **27**(3), p 131-139
8. S. Srikanth and K.T. Jacob, Vapour Pressure of Calcium Corresponding to the Reduction of Calcia by Aluminium, *Trans. Ind. Inst. Metals*, 1991, **44**(5), p 369-373
9. K.T. Jacob and S. Srikanth, Physical Chemistry of the Reduction of Calcium Oxide with Aluminium in Vacuum, *High Temp. Mater. Process.*, 1990, **9**, p 77-92
10. H. B. Bartl and T. Scheller, Zur Struktur Des 12CaO.$7Al_2O_3$, *N. Jb. Miner. Mh.*, 1970, **35**, p 547-552, in German
11. J. Jeevaratnam, F.P. Glassser, and L.S.D. Glasser, Anion Substitution and Structure of 12CaO.$7Al_2O_3$, *J. Am. Ceram. Soc.*, 1964, **47**(2), p 105-106
12. J.A. Imlach, L.S.D. Glasser, and F.P. Glassser, Excess Oxygen and the Stability of 12CaO.$7Al_2O_3$, *Cement Concrete Res.*, 1971, **1**(1), p 57-61
13. H. Hosono and Y. Abe, Occurrence of Superoxide Radical Ion in Crystalline 12CaO.$7Al_2O_3$ Prepared via Solid-State Reaction, *Inorg. Chem.*, 1987, **26**(8), p 1192-1195
14. K. Hayashi, M. Hirano, S. Matsuishi, and H. Hosono, Microporous Crystal 12CaO.$7Al_2O_3$ Encaging Abundant O^- Radicals, *J. Am. Chem. Soc.*, 2002, **124**(5), p 738-739
15. S.W. Kim, K. Hayashi, M. Hirano, and H. Hosono, Electron Carrier Generation in a Refractory Oxide 12CaO.$7Al_2O_3$ by Heating in Reducing Atmosphere: Conversion from an Insulator to a Persistent Conductor, *J. Am. Ceram. Soc.*, 2006, **89**(10), p 3294-3298
16. C. Greskovich and H. Schmalzried, Non-stoichiometry and Electronic Defects in Co_2SiO_4 and in $CoAl_2O_4$-$MgAl_2O_4$ Crystalline Solutions, *J. Phys. Chem. Solids*, 1970, **31**(4), p 639-646
17. E. Woermann and A. Muan, Phase Equilibria in the System CaO-Cobalt Oxide in Air, *J. Inorg. Nucl. Chem.*, 1970, **32**(5), p 1455-1459
18. B. Vazquez, L.M.T. Martinez, N. Alvarez, J.F. Vente, and P. Quintana, Sub-solidus Phase Equilibria in the System CaO-Al_2O_3 -CoO and the Crystal Structure of Novel $Ca_3CoAl_4O_{10}$, *J. Solid State Chem.*, 2002, **166**(1), p 191-196
19. K.T. Jacob and S.S. Pandit, Gibbs Energy of Formation of Cobalt Divanadium Tetroxide, *J. Solid State Chem.*, 1985, **60**(2), p 237-243
20. M.W. Chase, Jr. (Ed.), NIST-JANAF Thermochemical Tables, 4th ed., *J. Phys. Chem. Ref. Data*, 1998, Vol. 2, Monograph No. 9, p 1585, Am. Inst. Phys., USA
21. S. Mukhopadhyay and K.T. Jacob, Phase Equilibria in the System NiO-CaO-SiO_2 and Gibbs Energy of Formation of $CaNiSi_2O_6$, *Metall. Mater. Trans. A*, 1995, **26A**, p 2311-2315
22. S. Mukhopadhyay and K.T. Jacob, Phase Equilibria in the System CaO-CoO-SiO_2 and Gibbs Energies of Formation of the Quaternary Oxides, $CaCoSi_2O_6$, $Ca_2CoSi_2O_7$ and $CaCoSiO_4$, *Am. Mineral.*, 1996, **81**, p 963-972
23. H.K. Hardy, Sub-regular Solution Model and its Application to Some Binary Alloy Systems, *Acta Metall.*, 1953, **1**, p 202-209
24. K.T. Jacob and J.P. Hajra, Oxygen Content of Liquid Cobalt in Equilibrium with $CoO(1 + x)Al_2O_3$ and α-Al_2O_3, *Z. Metallkde.*, 1986, **77**, p 673-677
25. K.T. Jacob, Unpublished Research, 2007